Check for updates

View Article Online
View Journal

Nanoscale

Accepted Manuscript

This article can be cited before page numbers have been issued, to do this please use: C. Gomez, A. M. Silva, M. C. Strumia, L. Avalle and M. I. ROJAS, *Nanoscale*, 2017, DOI: 10.1039/C7NR02736B.

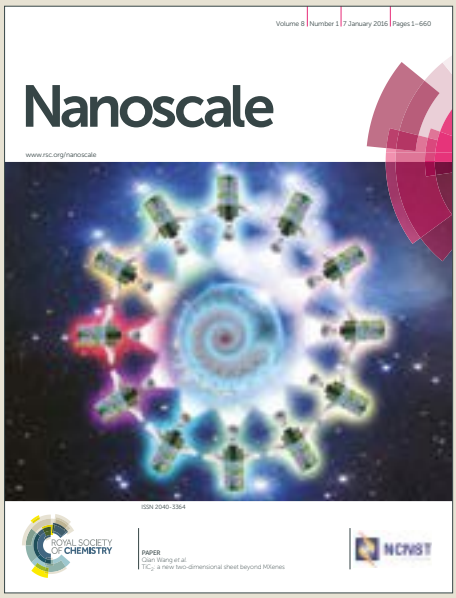

This is an Accepted Manuscript, which has been through the Royal Society of Chemistry peer review process and has been accepted for publication.

Accepted Manuscripts are published online shortly after acceptance, before technical editing, formatting and proof reading. Using this free service, authors can make their results available to the community, in citable form, before we publish the edited article. We will replace this Accepted Manuscript with the edited and formatted Advance Article as soon as it is available.

You can find more information about Accepted Manuscripts in the author guidelines.

Please note that technical editing may introduce minor changes to the text and/or graphics, which may alter content. The journal's standard Terms & Conditions and the ethical guidelines, outlined in our author and reviewer resource centre, still apply. In no event shall the Royal Society of Chemistry be held responsible for any errors or omissions in this Accepted Manuscript or any consequences arising from the use of any information it contains.

ROYAL SOCIETY OF CHEMISTRY

rsc.li/nanoscale

Please do not adjust margins

ROYAL SOCIETY OF CHEMISTRY View Article Online
DOI: 10.1039/C7NR02736B

Nanoscale

ARTICLE

The Origin of High Electrocatalytic Activity of Hydrogen Peroxide Reduction Reaction by g-C_3N_4/HOPG Sensor

AReceived 17th April 2017,
Accepted 00th June 2017

DOI: 10.1039/x0xx00000x

www.rsc.org/

C.G. Gomez,[a*] A. M. Silva[b] , M.C. Strumia[§,a], L.B. Avalle[c], M.I. Rojas[d†]

Graphitic carbon nitride (g-C_3N_4) was synthesized from a low-cost precursor by means of a thermal process. The product was characterized by several spectroscopic techniques and crystallinity was analyzed by X-ray diffraction. In the manufacture of the sensor, the g-C_3N_4 was chemically exfoliated and a film was placed on the surface of a Highly Oriented Pyrolytic Graphite (HOPG). We compared the electrocatalytic activities of g-C_3N_4/HOPG and pristine HOPG surfaces as sensors for H_2O_2 quantification in buffer solution at pH 7. Results indicate that the surface of g-C_3N_4/HOPG exhibits striking analytical stability as well as reproducibility, enabling a reliable and sensitive determination within 0.12 - 120 μM interval with a detection limit of 0.12 μM. These results suggest that this g-C_3N_4 film is a really particularly good nano-structured material to be applied as biosensor. Chemical and physical factors are responsible for the outstanding electrocatalytic activity observed. The N in the g-C_3N_4 allows huge uptake of H_2O_2 through hydrogen-bonding interaction and the change in the electronic structure since HOPG/g-C_3N_4 heterojunction favors the charge transference process through the interface.

Introduction

Graphitic materials are suitable for the manufacture of biosensors to quantify molecules of biological interest, due to their high specific surface area. Graphitic carbon nitride is a new class of carbonaceous material doped with N atoms[1-6]. Tri-s-triazine based-connection pattern is the most stable allotrope of g-C_3N_4 at ambient conditions[1-3]. Since N and C atoms belong to different groups of the periodic table, they form different numbers of bonds which, in the honeycomb lattice, gives rise to a periodic distribution of pores[7]. Since carbon nitride is mainly composed of C and N atoms, among the most abundant elements, it is also being considered an environmentally friendly material. It can be synthesized at low cost from polymerization of N-rich precursors like cyanamide, dicyandiamide and melamine,[3] obtaining a highly textured and graphitic organized polymeric material. The lattice parameter is 7.14 Å and the sheets are stacked with an interplanar distance of 3.25 Å [5-7]. As N and C atoms have different electronegativities, the C-N bonds are polar, where N is positively and C is negatively charged[7]. In reference to the electrical properties, it is an n-type organic semiconductor with an indirect band gap of 1.90 eV[7].

This N-doped carbonaceous material has a high electro-catalytic activity[8-10]. Taking into account its high sensitivity, good selectivity and ease operation, g-C_3N_4 may be used in the manufacture of sensor[4,11]. On the other hand, the H_2O_2 molecule is the product of several biological enzyme-catalyzed reactions and its detection and quantification play an important role in food industry, environmental protection and medical diagnoses[12-13]. Among the different techniques used to detect H_2O_2, the electrochemical method has the advantage of being simple, with low cost and great sensitivity as well as selectivity.

Electro-catalytic activity of HOPG and g-C_3N_4/HOPG surfaces for HPRR takes place, according to the following equation:

$$H_2O_2 + 2H^+ + 2e^- \leftrightarrow 2H_2O \quad (1)$$

Although the electrolyte has pH 7, the reduction of H_2O_2 (HPRR) is considered an acid medium since the reaction takes place on the cathode surface. Thus, there is a high [H^+] concentration at the interface, even though it is lower in the solution.

Recently, Rojas et al[14] have studied the H_2O_2 adsorption and its reduction on graphene by means of theoretical calculation. Adsorption energy was -0.051 eV (physisorption). The slow step was the cleavage of the O-O bond with an energy barrier of 1.00 eV for the Stone-Wale defective site[15] and 1.70 eV for normal site.

[§]IPQA-CONICET, [a]Departamento de Química Orgánica, Facultad de Ciencias Químicas, Universidad Nacional de Córdoba, Edificio Ciencias II, Haya de la Torre y Medina Allende, (5000) Córdoba, Argentina. *Dr. C.G. Gomez, Tel. +54 351 5353867 int. 53343, E-mail gom@fcq.unc.edu.ar.
[b]Divisão de Metrologia de Materiais, (INMETRO) Instituto Nacionalde Metrologia, Normalizacão e Qualidade Industrial, Duque de Caxias, Río de Janeiro, RJ 25245-020, Brazil.
[c]IFEG –CONICET, Facultad de Matemática, Astronomía, Física y Computación, Universidad Nacional de Córdoba, Ciudad Universitaria, (5000) Córdoba, Argentina.
[d]INFIQC–CONICET, Departamento de Química Teórica y Computacional, Facultad de Ciencias Químicas, Universidad Nacional de Córdoba – Ciudad Universitaria, 5000 Córdoba, Argentina. [†] Dra. M.I. Rojas, Tel. +54 351 5353853int. 55186. E-mail mrojas@fcq.unc.edu.ar.

Published on 14 July 2017. Downloaded by Cornell University Library on 14/07/2017 07:57:02.

Nanoscale Accepted Manuscript

Please do not adjust margins

View Article Online
DOI: 10.1039/C7NR02736B

Published on 14 July 2017. Downloaded by Cornell University Library on 14/07/2017 07:57:02.

The following mechanism of consecutive reaction involves two single electrochemical species, considered as follows:

$$O \xrightarrow{n_1 e} R_1 \xrightarrow{n_2 e} R_2 \quad (2)$$

The first step is a reductive H_2O_2 adsorption on the surface (*S*):

$$H_2O_2 + 1e^- + S \rightarrow (H_2O_2{}^-)_{ads}/S \quad (3)$$

It is followed by a reductive dissociation of H_2O_2:

$$1e^- + (H_2O_2{}^-)_{ads}/S \xrightarrow{SLOW} (2HO^-)_{ads}/S \quad (4)$$

Equation (4) is the rate-determining step for HPRR, due to the fact that O-O cleavage generally has an important energy barrier. Finally, adsorbed hydroxyl groups are protonated to give two desorbed water molecules:

$$(2HO^-)_{ads}/S + 2H^+ \xrightarrow{FAST} 2H_2O + S \quad (5)$$

The rate of equation (3) depends on the vacancies of surface sites, while the rate of equation (4) depends on the content of H_2O_2 adsorbed onto the surface.

On the surface of both kinds of electrodes, HPRR takes place through a mechanism involving (3-5) elementary steps. The catalytic activity of each surface depends on the energy barrier of the (4) step.

In this work, we performed the synthesis of g-C_3N_4 from a thermal process of a low-cost precursor such as melamine. This product was then characterized by spectroscopic techniques and crystallinity was analyzed by X-ray diffraction. After that, a g-C_3N_4 sample was chemically exfoliated and deposited on HOPG surface to be used as an electrochemical sensor. Finally, the surfaces of g-C_3N_4/HOPG and HOPG were tested by electrochemical techniques for quantification of low concentration of H_2O_2 in buffer solution at pH 7.

Experimental Details

Reagents and equipment

Reagents were used as purchased. Melamine > 99 wt.-% Merck, (Switzerland); H_2SO_4 98 wt.-%, Cicarelli (Argentina); $NaHCO_3$ p.a., Cicarelli (Argentina); 0.20 M phosphate buffer pH 7, Anedra (Argentina); HCl 37 wt.-%, Cicarelli (Argentina); ethanol 96 vol.-%, Porta (Argentina). H_2O_2 30 vol.-%, Cicarelli (Argentina).

Spectrophotometric measurements were recorded on a Shimadzu UV-Visible spectrophotometer UV -1800, UV Probe 2.30 (Japan).

Fourier-transform infrared (FTIR) spectra of samples were obtained by using a Nicolet iN10 spectrometer (USA).

Determination of pH was carried out by using a digital pH meter Altronix, TPXI 1584 (Argentina).

Transmission electron microscopy (TEM) was recorded by using a JEOL-JEM 1200 EXII instrument (USA).

Scanning Electron Microscopy of field emission gun (SEM-FEG) was recorded through a microscope SIGMA HD-CARLS ZEISS (Germany).

The X-Ray Diffraction (XRD) patterns were measured at room temperature on a PAN Analytical X-Pert Pro diffractometer (40 kV, 40 mA) in Bragg-Brentano geometry with Cu Ka radiation in the range of 10 to 100° with step size of 0.02° and a step counting time of 10s (Netherland).

The Dispersive X-ray Spectroscopy (EDS) was performed with an Energy Dispersive Spectrometer attached to the SEM, consisting of a silicon drift Oxford detector with an Aztec characterization system.

The electrochemical analyser was a Metrohm AUTOLAB-PGSTAT302N potentiostat (Switzerland) equipped with a staircase scan module and an electrochemical interface using the NOVA 2.01 software package.

Synthesis of g-C_3N_4 and Method

Allotrope of g-C_3N_4 constituted by polymer based-on tris-s-triazine units was successfully synthesized from of melamine thermal process using an electrical oven (Model 332 INDEF, Argentina). This reagent (8.00 g) was introduced into a porcelain cup and left into oven for reaction (Fig. 1). The thermal treatment used had a heating rate of 2 °C / min from 25 °C to 550 °C, kept constantly for 4 h.

Afterwards, the g-C_3N_4 was chemically exfoliated. A sample (0.20 g) of g-C_3N_4 synthesized was mixed with a 0.50 M H_2SO_4 aqueous solution (400 mL) and then left under sonication for 30 min, from which a yellow suspension was obtained (Fig. 1). After that this suspension was mixed with a 96 vol.-% ethanol in volume proportion (50:50) and the exfoliated g-C_3N_4suspension was precipitated by centrifugation at 7000 rpm.

Exfoliated g-C_3N_4 sample was suspended with 10 mL of an ethanol/water mixture (70:30) under sonication for 15 min, separated from supernatant by centrifugation. This process was performed three times. Finally, a 0.033 wt.-% g-C_3N_4 ethanol suspension after 20 min of sonication was attained and characterized by UV-Vis spectrometry.

In addition, one drop of g-C_3N_4 ethanolic suspension was seeded twice on the sample holder grid for TEM, then dried at 25°C. Similarly, a g-C_3N_4 sample was deposited on carbon tape / sample holder, then gold-plated and characterized by Scanning Electron Microscopy / Energy-Dispersive Ray-X Spectroscopy (SEM/EDS).

Fig 1 From precursor to polymer synthesis and chemical exfoliation process.

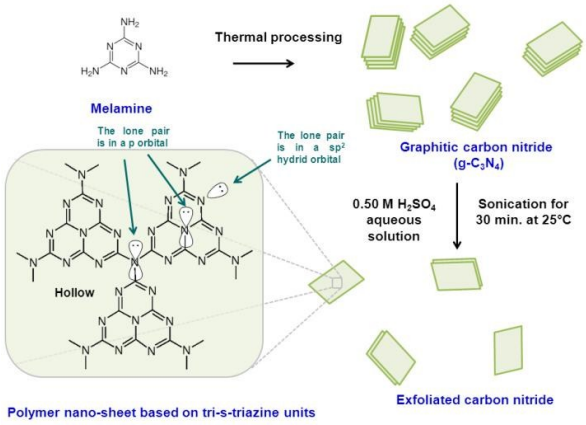

Nanoscale Accepted Manuscript

This journal is © The Royal Society of Chemistry 2017

View Article Online
DOI: 10.1039/C7NR02736B

Published on 14 July 2017. Downloaded by Cornell University Library on 14/07/2017 07:57:02.

Electrochemical Measurements

A conventional electrochemical cell of three electrodes was used, consisting of the working electrode, an Ag/AgCl reference electrode and a gold rod (Alfa Aesar 99.9985% purity) auxiliary electrode. The auxiliary electrode was cleaned by annealing in butane flame during 2 min, cooled under N_2 flux, and immediately placed in contact with the electrolytic solution. Oxygen-free solutions were obtained by continuously purging the electrochemical cell with nitrogen gas (99.999% purity). Water from a Milli-Q Millipore System was used for the preparation of all solutions and for glassware cleaning. All chemicals were of analytical grade. The working electrode used was a 7x7 mm^2 HOPG, mechanically exfoliated with the adhesive tape method. In the case of g-C_3N_4/HOPG surface, the film was placed by dripping g-C_3N_4 ethanolic suspension on HOPG surface (8 drops), followed by ethanol evaporation at 25 °C.

Cyclic voltammetry

The working electrodes were transferred to the electrochemical cell with a drop of ultrapure water. The measurements for blank experiments were performed in buffer pH 7 cycling in the range [-1, 0.4] V vs. Ag/AgCl reference electrode at 0.050 V/s. Different aliquots of 50 μL of a stock solution of the H_2O_2 analyte were injected in the 50 mL electrochemical cell to give various final H_2O_2 concentrations in the bulk solution. The potentiodynamic current density – potential (j-E) profiles were recorded after each addition under steady-state conditions.

Current transients

Stabilization of the system was performed by applying an initial potential, V_i, of -0.40 V. A potential step at a more negative potential value, V_{trans}, of -0.6 V was then applied recording the current as a function of time. Afterwards, the potential was returned to the initial value. This procedure allowed verifying the interface stability after a kinetic of potential variation was used. Voltammogram comparisons obtained under steady-state conditions before and after analyte addition were compared to determine V_{trans} value.

Impedance measurements

The amplitude of the *ac* perturbation signal was 10 mV and the frequency range scanned was 0.1 Hz – 100 KHz for HPRR at $-0.6\ V$ vs. Ag/AgCl as a reference electrode.

Model and Computations

The optimized lattice parameter for the g-C_3N_4/graphene bilayer was 7.29Å. The first sheet, the tri-s-triazine one, was composed of 8 N and 6 C atoms; the second sheet, the graphene one, had 18 C atoms. The atoms in both layers were arranged in a honeycomb lattice. The unit cell was tetrahedral of 7.29 Å x 7.29 Å x 30 Å with periodic boundary conditions at x, y, z directions imposed in order to represent an infinite surface.

All DFT calculations were performed using the Quantum Espresso package[16] with Van der Waals interactions. The Kohn-Sham orbitals and charge density were expanded in plane-wave basis sets up to a Kinetic Energy cutoff of 60 and 480 Ry for all atoms. Ultra soft pseudopotentials were employed with the Perdew-Burke-Ernzerhof approximation for exchange and correlation in the PBE functional[17-18]. The BZ was sampled with 4x4x1 irreducible Monkhorst-Pack k-point grid[19]. The convergence threshold for the total energy at each electronic calculation was set to $1x10^{-8}$ Ry. Geometry optimizations were performed employing the Broyden – Fletcher – Goldfarb-Shanno (BFGS) algorithm (for stress minimization) and total forces acting on each ion are minimized to reach less than $1x10^{-3}$ Ry/a.u. by movement of the ionic positions.

Results and Discussions

Synthesis and characterization of g-C_3N_4

Synthesis of g-C_3N_4 by thermal treatment of a low-cost precursor such as melamine was performed with a yield of 75wt. % at 550 °C for 4 h[3] (see Fig. 1). After that, a sample of synthesized g-C_3N_4 was characterized by spectroscopic techniques. Fig. 2 A) shows a photograph of a sample of g-C_3N_4 where, at first sight, this material is composed of yellow dust together with irregular particles of diameters near 3 mm and a low apparent density. These properties agree with those found in material reported by other authors[3-4]. In addition, Fig.2 B) shows a micrograph of SEM of an exfoliated g-C_3N_4 sample, where the surface is composed of staked nanosheets with the presence of terraces and steps.

Fig. 2 C) shows the profile of FTIR spectrum of a g-C_3N_4 sample, which exhibits different bands. The signal at 3250 cm^{-1} is attributed to stretching ν N-H, while that at 1630 cm^{-1} corresponds to ν C=C or ν C=N, these characteristic bands being typical of tri-s-triazine allotrope[20]. In addition, the flexion signal σ C-N of aromatic heterocyclic ring twisting appears at 805 cm^{-1}.

Fig. 3 shows the morphology and composition of a g-C_3N_4 crystal obtained by Energy Dispersive X-ray Spectroscopy (EDS). From the EDS analysis, it is found that C and N content mainly agrees with C_3N_4 formula. This graphite kind normally has a crystalline structure, which has been studied through X-ray diffraction patterns (XRD). The inter-layer distance can be experimentally determined through the angles at which the diffraction peak appears according to Bragg's Law[21]:

$$n\lambda = 2d \cdot \sin\theta \quad (6)$$

where $2d \cdot \sin\theta$ is the path difference between the two rays,

Fig. 2A) The photograph shows the texture of the yellow crystals of synthesized g-C_3N_4; **B)** SEM image shows the agglomerates of porous solids; **C)** FTIR: νN-H 3250 cm^{-1}, νC=C or νC=N 1630 cm^{-1} stretching and σC-N aromatic heterocyclic ring twisting 805 cm^{-1}.

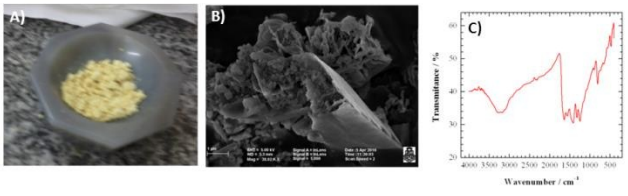

Nanoscale Accepted Manuscript

View Article Online
DOI: 10.1039/C7NR02736B

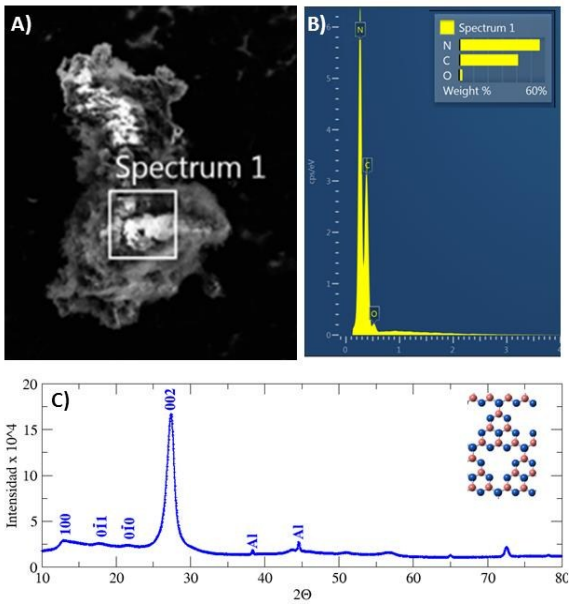

Fig. 3 Above) crystal morphology and EDS composition of g-C_3N_4 crystal synthesised. The square is of 10 µm of sideway. **Down)** X-ray diffraction pattern (XRD) shows a crystalline structure. The 002 plane is located at 27.4°, corresponding to inter-planar distance of 3.25 Å. Inset: Arrangement of atom in a layer, blue spheres are N atoms; red spheres are C atoms.

θ is the angle of incidence and the integer n is the order of the corresponding reflection peak.

Fig. 3 Down) shows the XRD pattern of g-C3N4 sample. The 002 peak appears at 27.4° corresponding to an inter-planar distance of 3.25 Å. The peak is that of the highest intensity and it is also sharp indicating that the synthesis product is crystalline. Low angles such as $100, 01\bar{1}; 0\bar{1}0$ are characteristic peaks of the tri-s-triazine structure[3-4,7,22-23] which depend on the arrangement of atoms in the layer. The inset of Fig. 3 shows the arrangement of atoms. Table 1 lists Miller indexes, angles at which the corresponding distance of the pattern observed are seen. In addition, other peaks are found, corresponding to the aluminium sample holder used in the characterization.

Table 1 Show hkl plane assignation, the angles, the plane distance and the material.

hkl	2Θ [°]	d [Å]	Material
100	12.9	6.83	g-C_3N_4
$01\bar{1}$	17.8	4.98	g-C_3N_4
$0\bar{1}0$	21.6	4.10	g-C_3N_4
002	27.4	3.25	g-C_3N_4
111	38.4	2.34	Al
	43.7	2.07	g-C_3N_4
200	44.6	2.03	Al
	50.9	1.79	g-C_3N_4
	56.8	1.62	g-C_3N_4
	65.0	1.43	g-C_3N_4
	72.5	1.30	g-C_3N_4
	78.2	1.22	g-C_3N_4

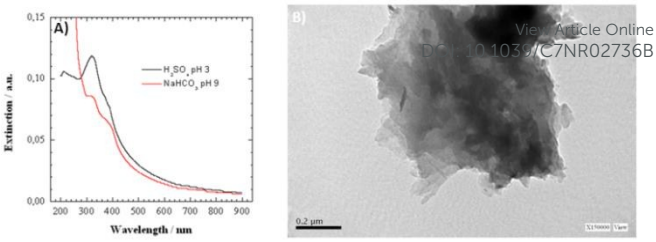

Fig. 4 g-C_3N_4 exfoliated. **A)** UV-Visible Spectroscopy and **B)** TEM image shows microcrystal of a few sheets of thickness.

Adsorption of g-C_3N_4 film on HOPG surface

g-C_3N_4 nanosheets were obtained from chemical exfoliation of synthesized product assisted by ultra-sonication (Fig. 1)[24-25]. The N atom in the structure in a 0.5 M H_2SO_4 aqueous solution was protonated, yielding sheets positively charged. These were repulsed with each other, which led to a chemical exfoliation accelerated by sonication. After that, exfoliated g-C_3N_4 nanosheets were placed onto HOPG surface from an ethanolic g-C_3N_4 suspension, drop by drop. Following ethanol evaporation, a g-C_3N_4 film was attained.

Fig. 4 A) exhibits the UV–Visible spectrum of an aqueous suspension of the exfoliated g-C_3N_4 at pH 3 and pH 9. The profile of spectral curves agrees with that found by Das et al[26], which supports the formation of g-C_3N_4. In both cases, two bands near 320 and 370 nm were observed, which was related to the existence of a conjugated π system.

This phenomenon supports the fact that the g-C_3N_4 polymer has an aromatic structure based on interconnected tri-s-triazine units where their atoms have sp^2 hybridization. Taking into account the different environments, three different types of N atoms were observed. A N atom, with lone pair electrons in a sp^2 orbital, and two different types of N atoms with a lone pair in p orbitals (Fig. 1).

Fig. 4 B) shows a micrography Transmission Electron Microscopy (TEM) for exfoliated g-C_3N_4, where micro-crystal of few sheets of thickness can be observed.

Cyclic Voltammetry (CV) and Chronoamperometry (CA)

We compared the electrochemical properties and performance of HOPG and g-C_3N_4/HOPG electrodes by CV and CA.

The CA $j(t)$-time response is related to the number of adsorption sites on the cathode surface taking into account the mechanism proposed and the kinetics for each step. In HPRR mechanism there are two reduction steps (3-4) followed by a protonation step (5) and a site release. Only the reduction steps (3-4) contribute to the cathodic $j(t)$. Thus, the $j(t)$ value responses to a potential step for HPRR, neglecting the double layer charging, can be approached as follows:

$$j(t) = n_1 F k_1\big(1-\theta(t)\big) + n_2 F k_2 \theta(t) \qquad (7)$$

Two terms of equation (7) have rate constants $k_1\big(\eta, C_{H_2O_2}\big)$ and $k_2\big(\eta, C_{H_2O_2}\big)$, which depend on the over-potential applied (η) and the H_2O_2 concentration$\big(C_{H_2O_2}\big)$ in the solution. Thus, kinetics of H_2O_2 adsorption (Eq. 3) depends on the number of free sites on the surface$(1-\theta(t))$, while cleavage of the O-O bond depends on the number of adsorbed molecules $\theta(t)$.

Published on 14 July 2017. Downloaded by Cornell University Library on 14/07/2017 07:57:02.
Nanoscale Accepted Manuscript

This journal is © The Royal Society of Chemistry 2017

Please do not adjust margins

View Article Online
DOI: 10.1039/C7NR02736B

Published on 14 July 2017. Downloaded by Cornell University Library on 14/07/2017 07:57:02.

The $j(t)$-time response, for a planar electrode surface is related to the $C_{H_2O_2}$ by means of the Cottrell equation[27], applied to a process diffusion-controlled process:

$$|j(t)| = nF\sqrt{\frac{D_O}{\pi}}t^{-1/2}C_{H_2O_2} \quad (8)$$

where *n* is the stoichiometric number of electrons involved in the reaction; F is Faraday's constant; $C_{H_2O_2}$ is the concentration of electroactive species; and D_O diffusion constant. It can be noticed that $|j(t)|$ falls as $t^{-1/2}$. From the slope of $|j(t)|$ vs. $t^{-1/2}$ plot, the diffusion coefficient D_O of the H_2O_2 in 0.2 M phosphate buffer is determined. D_O is equal to $(4.0 \pm 0.5) \cdot 10^{-6} cm^2 s^{-1}$. The value is slightly larger than that informed by Nasirizadehet al[28], who found a value of $2.34 \cdot 10^{-6} \frac{cm^2}{s}$ measured in a 0.1 M phosphate buffer.

Fig. 5 Left) shows the CV of the HOPG surface measured in a 0.2M buffer phosphate pH 7 vs. Ag/AgCl at a scan rate of 0.05 V/s. The black line corresponds to the blank voltammogram, which does not exhibit any redox peak. It shows the lowest current density within the potential interval [-1; -0.2] V. The coloured lines show the j-V profiles corresponding to successive injections of 50 µL of 10 mM of H_2O_2 to the electrochemical cell. If zoom is made between $[-1..-0.6]$ V, the green line shows $|j(t)|$value higher than the blank. Assays were performed within the $[12.48; 123.5]\mu M$ interval of H_2O_2 concentrations and the density current values observed are within the $[-200; -20]\mu A/cm^2$ interval.

Fig. 5-Right) shows $j(t)$ - time response of HOPG/electrolyte interface, at a potential applied of -0.6 V vs. Ag/AgCl in buffer pH 7, with the addition of 50 µL of 10 mM of H_2O_2. A detection limit of 12.5 µM of H_2O_2 is found within the 11.0 – 123.5 µM interval. At short times, where the double layer charging dominates, the transient profile presents a maximum which evidences a slow kinetics for the HPRR. The steady state conditions are reached close to 120 s. At longer times, the current density reaches the limited value (j_∞). The j_∞ correlates with the $C_{H_2O_2}$ according to equation (8). Inset Fig. 5 shows the lineal response in the range 12.5 - 123.5 µM fitted by linear regression giving the following equation:

$$|j(t)|\mu A/cm^2 = -0.06616 + 0.06167 \cdot (C_{H_2O_2}\mu M) \quad (9)$$

Fig. 6-Left) shows the CV of g-C_3N_4/HOPG surface measured in 0.2M buffer pH 7 vs. Ag/AgCl at 0.05 V/s. The black line corresponds to the blank voltammogram; it exhibits the lowest current density within the [-1; 0.4] V potential interval. The coloured lines show the j-V profiles corresponding to successive injections of 50 µL H_2O_2 to the electrochemical cell. Small amounts of H_2O_2 produce significant changes in the voltammogram.

Fig. 6-Right) shows $j(t)$ - time response of HOPG/g-C_3N_4/electrolyte interface at a potential applied of -0.6 V vs. Ag/AgCl in buffer pH 7. The shape of the pulse is different to the HOPG one. It corresponds to a fast kinetics of HPRR. The steady state conditions were reached close to 50 s.

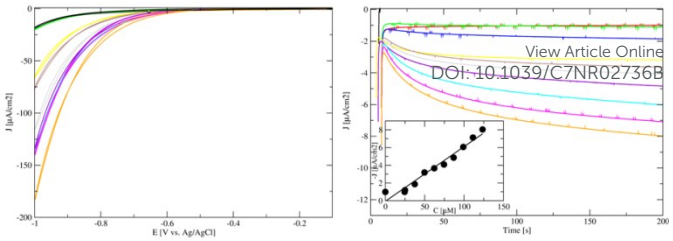

Fig. 5 HOPG graphite working electrode in 0.2M phosphate buffer pH 7 (Anhedra) **Left)** Current density – potential (j-V) profiles within [-1; 0] V potential interval vs. Ag/AgCl reference electrode with a scan rate of 0.05 V/s. **Right)** Current – time curve with successive addition of H_2O_2. The inset is the calibration curve at applied potential: -0.6 V, illustrating the electrode response to H2O2 addition. (black line) 0.2M buffer pH7; (red line) 12.48µM; (green line) 24.94µM ; (blue line) 37.36µM; (yellow line) 49.75 µM; (brown line) 62.11 µM; (grey line) 74.44 µM; (violet line) 86.74 µM; (light blue line) 99.01 µM; (magenta line) 111.25 µM; (orange line) 123.46 µM of H_2O_2 added, respectively.

The effect of $C_{H_2O_2}$ within the $[0.05; 118]\mu M$ interval was studied. First, we added successive injections of 50 µL of 0.1 mM H_2O_2 until 12.0 µM and then successive injections of 50 µL of 10 mM of H_2O_2. A detection limit of 0.12 µM was found.

It was surprising to find two linear behaviour regions. Inset Fig.6 shows the two $j(t)$ - time linear responses corresponding to [0.12; 48.31] µM and [60.22; 118] µM concentration intervals and the linear regression fittings:

$$\log(|j(t)|\mu A/cm^2) = 1.02088 + 0.02428 \cdot \log(C_{H_2O_2}\mu M) \quad (10)$$

$$\log(|j(t)|\mu A/cm^2) = -2.12595 + 2.00714 \cdot \log(C_{H_2O_2}\mu M) \quad (11)$$

Tian et al[4] studied a similar system, where an ultrathin g-C_3N_4 nanosheet adsorbed on a glassy carbon electrode (g-C_3N_4/GCE) was analysed within a higher concentration interval between 0 to 90mM of H_2O_2. Therefore, they did not find the first linear response at low concentration as in equation (10). Nitrogen-doped carbonaceous material, like g-C_3N_4/GCE[4] or N-doped carbon nanotubes on glassy carbon electrode (NCNT/GCE)[11], exhibits higher electrocatalytic performance than carbonaceous material. Here, at steady-state condition, the g-C_3N_4/HOPG electrode exhibits $j(t)$ within [-250.23; -22.86] $\mu A/cm^2$ interval for [0.12; 120] µM of H_2O_2, while HOPG electrode has lower $j(t)$within [-2.28; -0.28] $\mu A/cm^2$ interval for [12.0; 123.5] µM of H_2O_2.

Fig. 6 g-C_3N_4/HOPG graphite working electrode in 0.2M phosphate buffer pH 7 (Anhedra) **Left)** Current density – potential profiles within [-1; 0.36] V potential interval vs. Ag/AgCl reference electrode recorded at 0.05 V/s scan rate. **Right)** Current – time curve with successive addition of H_2O_2 to the 0.2 M buffer of pH 7. The inset is the calibration curve at applied potential: -0.6 V, illustrating the electrode response to H_2O_2 addition. (black line) 0.2M buffer pH7; (red line) 0.12 µM; (green line) 12.26 µM ; (blue line) 24.33 µM; (yellow line) 36.35 µM; (brown line) 48.31 µM; (grey line) 60.22 µM; (violet line) 72.06 µM; (light blue line) 83.85 µM; (magenta line) 95.58 µM; (orange line) 118 µM of H_2O_2 added, respectively.

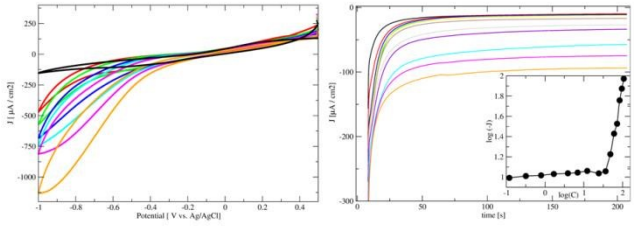

Nanoscale Accepted Manuscript

Please do not adjust margins

View Article Online
DOI: 10.1039/C7NR03756B

The transient in the double-layer regions of HOPG and g-C_3N_4/HOPG interfaces was remarkably different. Therefore, in the next section, by means of Electrochemical Impedance Spectroscopy, we studied the structures and charge transfer processes which take place through the interfaces.

Although all the measurements were carried out with N_2 bubbling, where O_2 is completely eliminated from the electrolyte, a brief discussion of the effect of O_2 dissolved was also included. As expected, O_2 reduction reaction (ORR) competes with HPRR at the potential studied. The ORR involves transfer of $4e^-$ according to:

$$O_2 + 4e^- + 4H^+ \rightarrow 2H_2O \quad (12)$$

Thus there are four elementary reduction steps:

$$O \xrightarrow{n_1 e} R_1 \xrightarrow{n_2 e} R_2 \xrightarrow{n_3 e} R_3 \xrightarrow{n_4 e} R_4 \quad (13)$$

Between each of these steps, a protonation step occurs according to the following mechanism described:

$$O_2 + 1e^- + surface \rightarrow (O_2{}^-)_{ads}/surface \quad (14)$$

$$(O_2{}^-)_{ads}/surface + 1H^+ \rightarrow (HO_2)_{ads}/surface \quad (15)$$

$$(HO_2)_{ads}/surface + 1e^- \rightarrow (HO_2^-)_{ads}/surface \quad (16)$$

$$(HO_2^-)_{ads}/surface + 1H^+ \rightarrow (O)_{ads}/surface + H_2O \quad (17)$$

$$(O)_{ads}/surface + 1e^- \rightarrow (O^-)_{ads}/surface \quad (18)$$

$$(O^-)_{ads}/surface + 1H^+ \rightarrow (HO)_{ads}/surface \quad (19)$$

$$(HO)_{ads}/surface + 1e^- \rightarrow (HO)_{ads}^-/surface \quad (20)$$

$$(HO)_{ads}^-/surface + 1H^+ \rightarrow surface + H_2O \quad (21)$$

Fig. 7 shows the effect of O_2 present on the voltammogram. The black line corresponds to $|j(t)|$ – potential profile of g-C_3N_4/HOPG graphite working electrode in 95.58 μM H_2O_2 + 0.2M phosphate buffer pH 7 without O_2; the red line corresponds to 3 min of O_2 bubbling. It was observed that the reduction current increases due to the presence of O_2. Both reactions (HPRR and ORR) occur simultaneously at the cathode. The green line was recorded after 22 min. bubbling of O_2 and exhibited the higher reducing current found. At longer O_2 bubbling times, no change was observed in the voltammogram profiles. Rojas et al.[29] studied the ORR of different electrodes. It is also an interesting reaction, but in this work there were no more results presented.

Electrochemical Impedance Spectroscopy measurements (EIS)

The EIS allows the study and characterization of interfaces and charge transfer processes that take place through them[24-25]. To obtain information, the results were fitted using an equivalent circuit model. In the case of HOPG/electrolyte interface, one Randle's circuit was employed while in the case of HOPG/g-C_3N_4/electrolyte interfaces, two Randle's circuits in series were used to emulate the cathode response.

One of the Randle's circuits emulates the response of the interface, including the Ohmic resistance of the solution (R_s), double layer response by means of a Constant Phase Element (CPE_1) and charge transfer resistance (R_1). When the film was present, a second Randle's circuit was employed. The R_2 and CPE_2 elements describe the film response.

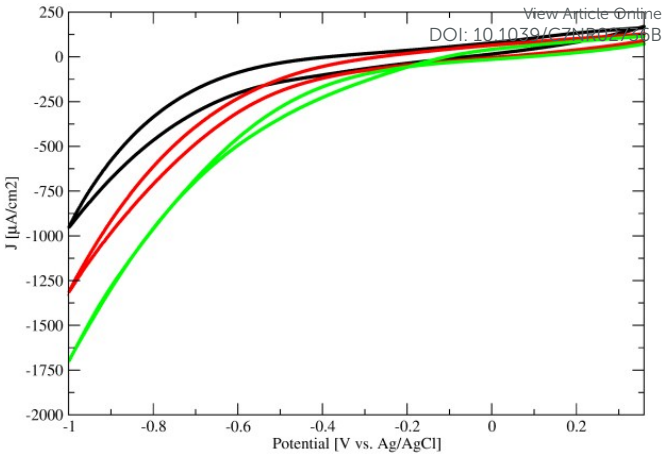

Fig. 7 Current density – potential profiles within [-1; 0.36] V potential interval vs. Ag/AgCl reference electrode recorded at 0.05 V/s scan rate employing g-C_3N_4/HOPG graphite working electrode. (black line) 95.58μM H_2O_2 in 0.2 M buffer of pH 7 with N_2 bubble; (red line) 95.58μM with 3 min. of O_2 bubble; (green line) 95.58μM with 22 min. O_2 bubble of H_2O_2 added to 0.2M phosphate buffer pH 7, respectively.

The transfer function of the equivalent circuit employed[25-26] can be expressed as:

$$Z(\omega) = R_s + \sum_{j=1}^{k} \frac{R_j}{1 + (i\omega)^{n_j} R_j Q_j} \quad (22)$$

where R_s, R_j and Q_j represent Ohmic resistance; resistance and differential capacity, respectively. CPE parameters n_j and Q_j are independent from the frequency. If n_j is close to 1, the element behaves as an ideal capacitor; if n_j is close to 0.5, it represents a diffusion process through the film; and if n_j approaches to zero, the film has a resistive response. Whenever $n_j < 1$, it indicates that the surface presents heterogeneity[30]. k is the number of Randle's circuits in series (1 or 2). The transfer function given by equation (22) comprises k time-constants$(\tau_j = R_j Q_j)$.

As the cathode is the negatively charged electrode, in the inner Helmholtz region, there are counter-cations aligned along the electrified surface and water molecules. In the outer Helmholtz region, there are cations, anion and solvent molecules which are also present in the diffusion layer.

Electrons are transferred across the electrified interface. The charge transfer leads to both Faradaic and non-Faradaic processes. The Faradaic component arises from the electron transfer of HPRR across the interface by overcoming an appropriate activation barrier, namely the total resistance[31].

Fig. 8 shows EIS measurements obtained for both interfaces in buffer pH 7. Fig. 8 left displays the Bode plot of HOPG/electrolyte interface, which is a highly ordered surface, thus CPE_1 elements tend to an ideal capacitor response with n value close to 1.

Fig. 8 right shows the Bode plot of the HOPG/g-C_3N_4/electrolyte interface, which evidences two-time constants, one can be related to the heterogeneity attribute to the presence of the film deposited on the surface; the other represents the double layer. The Bode plot of HOPG/electrolyte shows high values of the impedance module compared to that of the HOPG/g-C_3N_4/electrolyte interface.

Published on 14 July 2017. Downloaded by Cornell University Library on 14/07/2017 07:57:02.

Nanoscale Accepted Manuscript

This journal is © The Royal Society of Chemistry 2017

Please do not adjust margins

View Article Online
DOI: 10.1039/C7NR02736B

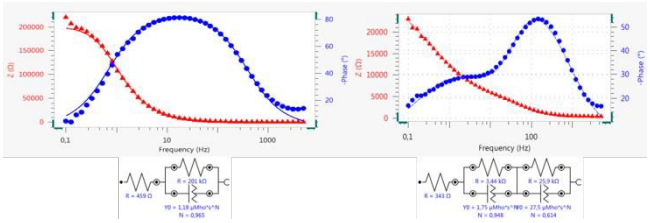

Fig. 8 Bode plot of EIS at -0.6 V vs. Ag/AgCl reference electrode of **Left)** HOPG/electrolyte interface buffer pH 7, **Right)** HOPG/g-C_3N_4/electrolyte interface buffer pH 7. **Down)** Equivalent circuits employed in the fitting.

HOPG/electrolyte		HOPG/g-C_3N_4/electrolyte	
R_s	459±8 Wcm^2	R_s	342±9 Wcm^2
R_1	201±4 KWcm^2	R_1	3.4±0.3 KWcm^2
CPE_1	Q_1 = 1.18±0.03mW^{-1}cm^{-2} n_1 = 0.965±0.005	CPE_1	Q_1 = 1.7±0.2mW^{-1}cm^{-2} n_1 = 0.95±0.03
		R_2	25±1 KWcm^2
		CPE_2	Q_2 = 27.5±0.9mW^{-1}cm^{-2} n_2 = 0.61±0.02

Table 2 Fitting parameters with equivalent circuits of the EIS measured in buffer pH 7, respectively.

Table 2 lists the fitting parameters obtained with the equivalent circuits for both interfaces. The R_s values are similar for both electrodes. The R_1 value is lower for the HOPG/g-C_3N_4/electrolyte interface while Q_1 and n_1 remain almost constant. The exponent n_1 tends to a capacitive behavior, whereas n_2 indicates diffusion process i.e., approaching a value of 0.5[28].

Fig. 9 shows the interfaces in the presence of H_2O_2 at a potential where the Faradaic process of HPRR takes place, evidencing changes in the Bode plots as well as in those parameters of components of the equivalent circuit, listed in Table 3. The impedance module decreases with the addition of H_2O_2, which shows that the response of the interface is sensitive to the H_2O_2 concentration. Fig. 9 – left shows the Bode plot of HOPG/electrolyte interface with only one-time constants, while Fig. 9 – right shows corresponding Bode plot of HOPG/g-C_3N_4/electrolyte interface. In this case, there are two-time constants which are not evident, $(\tau_1 = R_1Q_1)$ and $(\tau_2 = R_2Q_2)$, and can be detected from the circuit fitting. Therefore, one of the time-constants is associated with electron transfer process through g-C_3N_4 film and the other with the double layer region, according to the electron transfer steps described for HPRR (equations 3-5) which involve the surface.

We know that g-C_3N_4 is a semiconductor material with a band gap of 1.90 eV[7]; hence, surprisingly, when the film was present, we found a decrease in the total resistance and a shift in time constant with the increase of H_2O_2 concentration.

Fig. 10 - left shows that the total resistance is equal to $R_{Total}^{HOPG/elect.} = R_1$ or $R_{Total}^{HOPG/g-C_3N_4/elect.} = R_1 + R_2$ obtained from the fitting of the experimental data as a function of H_2O_2 concentration.

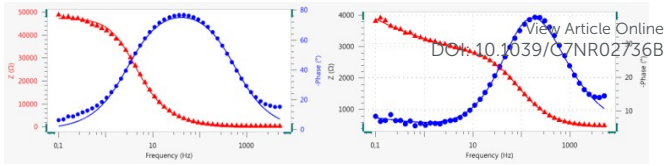

Fig. 9 Bode plot of EIS at -0.6 V vs. Ag/AgCl reference electrode of **Left)** HOPG/electrolyte interface buffer pH 7 + 86.74 μM H_2O_2, **Right)** HOPG/g-C_3N_4/electrolyte interface buffer pH 7 + 82.64 μM H_2O_2.

HOPG/electrolyte		HOPG/g-C_3N_4/electrolyte	
R_s	341±7Ω cm^2	R_s	323±9 Ωcm^2
R_1	47.2± 0.7KΩ cm^2	R_1	2.02±0.08 KΩcm^2
CPE_1	Q_1 = 1.36± 0.05μΩ^{-1}cm^{-2} n_1 = 0.942± 0.006	CPE_1	Q_1 = 2.171±0.2μΩ^{-1}cm^{-2} n_1 = 0.91±0.02
		R_2	18.37±0.08 KΩcm^2
		CPE_2	Q_2 = 639.3±0.2μΩ^{-1}cm^{-2} n_2 = 0.24±0.02

Table 3 Fitting parameters with equivalent circuits of the EIS measured in buffer pH 7 with the addition of 86.74μM of $H_2O_2$and 82.64 μM of H_2O_2, respectively.

In the case of $R_{Total}^{HOPG/elect.}$, the charge transfer went through a maximum between 10 and 50 μM of H_2O_2. Afterwards, resistance decreased with the increase in H_2O_2 concentration. Although the HOPG / g-C_3N_4 / electrolyte interface also exhibited a maximum at low concentrations, in the interval between 10 and 50 μM, the $R_{Total}^{HOPG/g-C_3N_4/elect.}$ values were lower than those of $R_{Total}^{HOPG/elect.}$ over the entire range of concentration, indicating that this surface was more electro-active than the other. When the g-C_3N_4 film was present, two features were observed: the effective barrier to charge transfer through the interface was diminished; at high concentration of H_2O_2, resistance reached a constant value of 20 KΩcm^2, showing that the electrode response was improved by the presence of g-C_3N_4 film.

Fig. 10 left) Total charge transfer resistance values; **right top** and **down)** constant face elements normalized to saturation value as a function of H_2O_2 concentration. Q_1 and Q_2 are the differential capacitances of the double layer and the film, respectively; **right middle)** continuous line: n_1 exponent; (**slash line**) n_2 exponent. (**blue**) HOPG/electrolyte and (**red**) HOPG/g-C_3N_4/electrolyte interfaces (**red** and **white**) correspond to n_2 or Q_2.

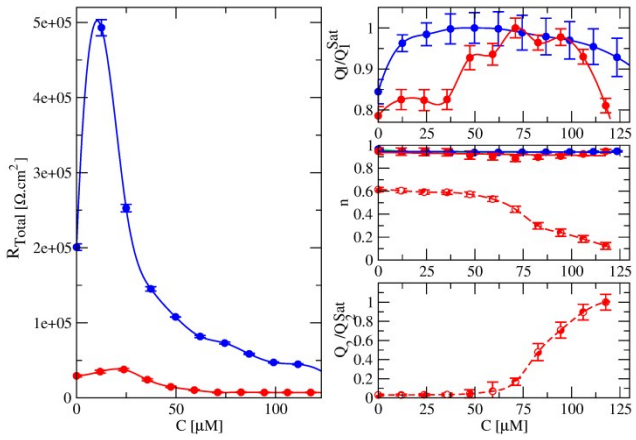

Published on 14 July 2017. Downloaded by Cornell University Library on 14/07/2017 07:57:02.

Nanoscale Accepted Manuscript

Please do not adjust margins

View Article Online
DOI: 10.1039/C7NR02736B

Published on 14 July 2017. Downloaded by Cornell University Library on 14/07/2017 07:57:02.

Fig. 10 – right top shows the constant phase element CPE_1 which describes the double layer response as a function of the analyte concentration. The Q_1 parameter starts decreasing after 50 μM and 75 μM for HOPG/electrolyte and HOPG/g-C_3N_4/electrolyte interfaces, respectively. The red line shows Q_1 fluctuations in the double layer behavior, due to periodic pore distribution and inhomogeneity present in the film. From the region between 37 and 80 μM of H_2O_2, Fig. 10 – right middle shows, for both interfaces, n_1 parameters close to 1, indicating a capacitive response of the CPE_1 elements. "**Red** and **white**" circle describes the n_2 parameter of the CPE_2 element. It changes from 0.6 to 0.2 according to concentration. At low concentration, the response is related to diffusion with deviations from Fick's second law[32]. Probably the analyte also diffuses through the film pores. At high concentration, the n_2 element approaches 0.2 indicating that the CPE_2 represents distorted resistance. Fig. 10 – right down shows the Q_2 parameter of the CPE_2 element as a function of concentration. Q_2 starts increasing at concentrations higher than 75 μM of H_2O_2 in the same region where n_2 parameter changes from diffusion to a resistive behaviour.

The n_2 and Q_2 parameters of the CPE_2 element were function of the concentration showing the electrochemical behaviour of the film at the HOPG/g-C_3N_4/electrolyte interface. The result shows changes in the charge transfer process on the interface which explains the two slopes observed in the calibration curve shown in Fig.6.

Why is the g-C_3N_4/HOPG sensor more electro-catalytic than the HOPG one?

As previously mentioned, all the atoms in the g-C_3N_4 structure have sp^2 hybridization, which allows a graphite structure of stacked sheets. This material is an n-type organic semiconductor with a band gap of 1.90 eV[7], whose Fermi level is close to the conduction band. Graphite has a band gap of 0.15 eV[7]; however, under certain environments, it behaves like a metal, due to its almost metallic character[33-35]. From the point of view of chemocatalysis, XH Li et al[33-34] analysed the Mott-Schottky effects that modify the electronic structure of the heterojunction HOPG/g-C_3N_4 through the bending of the bands. This phenomenon favours the charge transfer for the oxidation or reduction reactions. Recently, X Li et al[32] studied the graphene/g-C_3N_4 heterojunction, finding a considerable opening in the band gap, between 0.041 eV to 0.108 eV depending on sheet stacking. These band gaps are even smaller than those observed in graphite. Fig. 11 right shows the HPRR through the interface described according to the Gerisher model[31]. The g-C_3N_4 Fermi level (E_f) is near the conduction band. When a negative potential is applied to the electrode, the E_f is shifted until the redox potential $\left(E^0_{redox}\right)$ is reached, the analyte reduction begins and the semiconductor bands bend. This phenomenon favors the reaction at the g-C_3N_4/electrolyte interface. In graphite the reduction also occurs, however, $|j(t)|$ values were significantly lower. The reaction was more impeded due to lower H_2O_2 uptake on HOPG.

Fig. 11 left shows a scheme of the H_2O_2 adsorptions on HOPG / g-C_3N_4/ electrolyte interface.

The origin of the surprising selectivity and electrocatalytic activity of the g-C_3N_4/HOPG sensor is attributed to the chemical nature of tri-s-triazine units. The g-C_3N_4 sheets comprise N atoms which, unlike C atoms, have a lone electron pair. In g-C_3N_4 structure, there are three types of N atoms with different environments: those with lone pair in a sp^2 orbital and those with a lone pair in a p orbital[37] (Fig. 1). This feature allows the surface a huge uptake of H_2O_2 molecules through hydrogen bonding. This is a major advantage over graphite or graphene where H_2O_2 adsorption is more impeded and C atoms should lose part of their sp^2 hybridization and their aromatic character to allow adsorption, displaying particularly low adsorption energy values -0.05 eV[14].

We performed some calculation at a DFT level to study H_2O_2 adsorption on g-C_3N_4/graphene bilayer. Table 4 lists $E_{ads}^{g-C_3N_4/graphene}$ values. They are significantly higher than those reported for graphene[14]. The preferential site corresponds to N_2 with an energy value of -0.86 eV. In order to calculate coverage (Θ) and surface concentration(C_s), equilibrium conditions at the surface were assumed: $\mu_{sol}^{H_2O_2} = \mu_{ad}^{H_2O_2}$.

In order to have a rough estimation, only the translational contribution to $\mu_{sol}^{H_2O_2}$ is considered, and a non-interacting lattice gas adsorbed was assumed at the coverage Θ[38].

$$-kTln\left[\left(\frac{2\pi mkT}{h^2}\right)^{3/2}\frac{V}{N}\right] = kTln\left(\frac{\theta}{1-\theta}\right) + \mathrm{E}_{ads} \quad (23)$$

where k denotes Boltzmann constant, m the mass of the molecule, $C_{H_2O_2} = V/N$ and h the Planck constant. θ can be obtained from equation (23):

$$x = \exp\left(\frac{\mu_{sol}^{H_2O_2} - E_{ads}}{kT}\right) \quad (24)$$

Fig. 11 Left) Scheme of the H_2O_2 reduction reaction onto HOPG / g-C_3N_4/ electrolyte interface. **Right)** Gerisher's model for reduction reaction at the electrochemical interface. E_f ,E^0_{redox}, D_{Ox}, D_{Red} are Fermi level, redox potential, state distribution of oxidized and reduced species, respectively. **Down)** N_1, N_2, N_3 are the different adsorption sites. C: yellow sphere; N: gray sphere; O: red sphere; H: light blue sphere.

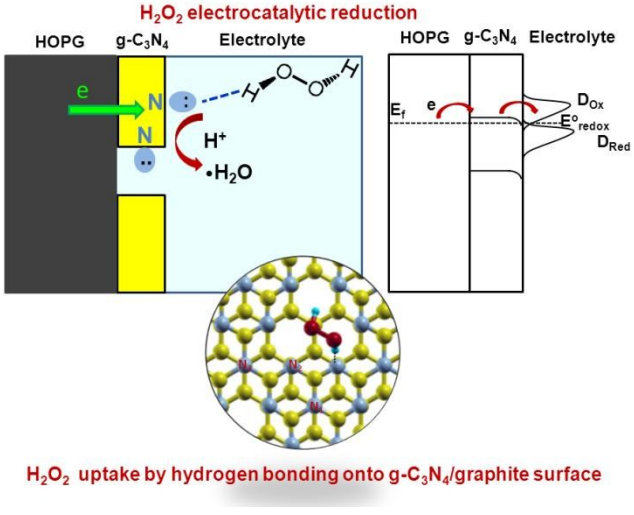

Nanoscale Accepted Manuscript

This journal is © The Royal Society of Chemistry 2017

View Article Online
DOI: 10.1039/C7NR02736B

Site	Q_N [a.u.]	E_{ads} [eV]	Lone pare
N_1	0.218	-0.80	p
N_2	0.262	-0.86	sp^2
N_3	0.452	-0.69	p

Table 4 Adsorption of H_2O_2 on g-C_3N_4/graphene surface. Site type, Mulliken atomic charge [atomic unit], adsorption energy [eV], lone pair.

$C_{H_2O_2}$ [μM]	HOPG		g-C_3N_4/HOPG	
	Θ	$C_s^{3/2}/C_{H_2O_2}$	Θ	$C_s^{3/2}/C_{H_2O_2}$
0.12	2.65×10^{-12}	2.19×10^{-15}	0.9925	349
12.00	2.65×10^{-10}	2.19×10^{-14}	0.9999	3.49
120.00	2.65×10^{-9}	6.93×10^{-14}	0.9999	0.35

Table 5 Coverage degree (Θ) and radio $C_s^{3/2}/C_{H_2O_2}$, where C_s is the surface concentration of adsorbed molecules, gives a measure for the enhancement of the local concentration of analyte due to the presence of the surface.

$$\theta = \frac{x}{1+x} \quad (25)$$

Table 5 shows the $C_s^{3/2}/C_{H_2O_2}$ radio, C_s and $C_{H_2O_2}$ the surface and bulk concentration, respectively. This radio should give an idea of the adsorption extent at each bulk concentration. We can see that E_{ads} difference gives HOPG a lower coverage, while for g-C_3N_4/HOPG, the surface is covered almost completely. On the other hand, θ and C_s are sensitive to $C_{H_2O_2}$, also seen in the transients of Figs. 5 and 6.

Conclusions

The aim of the present work was to develop an efficient green biosensor for the detection and quantification of H_2O_2. A comparative study between HOPG and g-C_3N_4/HOPG sensors was carried out. g-C_3N_4/HOPG electrode has the best electro-active performance for H_2O_2 quantification.

First, graphitic carbon nitride was synthesized from heat treatment of melamine. The product was tri-s-triazine polymer, one of the g-C_3N_4 allotropes, obtained with a yield of 75 wt. %. The g-C_3N_4 was characterized by spectroscopic techniques. Composition was evaluated by EDS and crystallinity by XRD diffraction, which supported the fact that tri-s-triazine-based-connection patterns were obtained. In order to form the g-C_3N_4 ultrathin film on the HOPG surface, g-C_3N_4 was successfully exfoliated in an acid medium under sonication; an ethanolic suspension was then prepared with them. Finally, the film was grown drop-wise from that suspension.

In the electrochemical characterization of the sensor, $j(t)$-time curves were performed at -0.6 V vs. Ag/AgCl reference electrode, in the range of low H_2O_2 concentration by means of successive addition.

For g-C_3N_4/HOPG sensor, we found a higher electro-catalytic activity and a lower detection limits compared to those seen in the HOPG one. The g-C_3N_4/HOPG electrode reached faster the steady state condition than the HOPG one, with different qualitative and quantitative behaviour. Particularly, the g-C_3N_4/HOPG sensor has analytical stability, reproducibility, allowing reliable and sensitive determination of low H_2O_2 concentration until a detection limit of 0.12 μM.

EIS measurements were also performed at a potential of $-0.6\ V$ where the Faradaic process of HPRR took place. For the entire range of concentrations studied, at the HOPG sensor, the reaction occurred with a higher charge transfer resistance than that at the g-C_3N_4/HOPG sensor.

This behavior is associated with the chemical and physical properties of the sensor. The g-C_3N_4/HOPG surface, due to N content, allows high uptake of H_2O_2. Heterojunction leads to a change in the electronic structure which favors the charge transference process through the bending of the bands.

This is the first study conducted in depth. With all the results shown, we can affirm that g-C_3N_4/HOPG is an efficient, low-cost and environmentally friendly sensor for H_2O_2 quantification. It allows an accurate and efficient determination of low H_2O_2 concentration.

For g-C_3N_4/HOPG sensor, we found a higher electro-catalytic activity and a lower detection limit compared to those observed in the HOPG one. The g-C_3N_4/HOPG electrode reached faster the steady state condition than the HOPG one, with different qualitative and quantitative behaviour. Particularly, the g-C_3N_4/HOPG sensor has analytical stability and reproducibility, allowing reliable and sensitive determination of low H_2O_2 concentration until a detection limit of 0.12 μM.

EIS measurements were also performed at a potential of $-0.6\ V$ where the Faradaic process of HPRR took place. For the entire range of concentrations studied, at the HOPG sensor, the reaction occurred with a higher charge transfer resistance than that at the g-C_3N_4/HOPG sensor.

This behavior is associated with the chemical and physical properties of the sensor. The g-C_3N_4/HOPG surface, due to N content, allows high uptake of H_2O_2. Heterojunction leads to a change in the electronic structure and favors the charge transference process through the bending of the bands.

This is the first study conducted in depth. With all the results shown, we can affirm that g-C_3N_4/HOPG is an efficient, low-cost and environmentally friendly sensor for H_2O_2 quantification. It allows an accurate and efficient determination of low H_2O_2 concentration.

Acknowledgements

This work was supported by CONICET PIP-11220120100031, PIP-11220110100499, PIP-11220100100411, PIO-15920150100013CO and SeCyT-UNC. A.M. Silva would like to thank INMETRO for postdoctoral fellowship. The authors also wish to thank language assistance by C. Mosconi.

Notes and references

1 M. Groenewolt, M. Antonietti, *Adv. Mater.*, 2005, **17**, 1789-1792.
2 B. Jürgens, E. Irran, J. Senker, P. Kroll, H. Müller, W. Schnick, *J. Am. Chem. Soc.*, 2003, **125**, 10288-10300.
3 A. Thomas, A. Fischer, F. Goettmann; M. Antonietti, J. Oliver Müller, R. Schlögl and J.M. Carlsson, *J. Mater.Chem.*, 2008,**18**, 4893-4908.

Published on 14 July 2017. Downloaded by Cornell University Library on 14/07/2017 07:57:02.

Nanoscale Accepted Manuscript

View Article Online
DOI: 10.1039/C7NR02736B

Published on 14 July 2017. Downloaded by Cornell University Library on 14/07/2017 07:57:02.

4 J. Tian, Q. Liu, C. Ge, Z. Xing, A.M. Asiri, A. O. Al-Youbi and X. Sun, *Nanoscale*, 2013, **5**, 8921-8924.
5 D.M. Teter, R.J. Hemley, *Science*, 1996, **271**, 53-55.
6 M.E. Straumanis, *J. Appl. Phys.*, 1959, **30**, 1965-1969.
7 A.M. Silva, M.I. Rojas, *Computational and Theoretical Chemistry*, 2016, **1098**, 41-49.
8 M. Ovcharov, N. Schcheerban, S. Filonenko, A. Mishura, M. Skoryk, V. Shvalagin, V. Granchak, *Material Science and Engineering: B*, 2015, **202**, 1-7.
9 S.N. Guo, Y. Zhu, Y.Y. Yan, Y.L. Min, J.C. Fan, Q. Xu, *Applied Catalysis B: Environmental*, 2016, **185**, 315–321.
10 F. Goettman, A. Fischer, M. Antonietti, A. Thomas, *Chem. Commun.*, 2006, 4530-4532.
11 X. Xu, S. Jiang, Z. Hu, S. Liu, *ACS Nano*,2010, **4**, 4292-4298.
12 P. Du, P. Wu, C. Cai, *Journal of Electroanalytical Chemistry*, 2008, **624**, 21-26.
13 J. Wang, *Chem. Rev.*, 2008,**108**, 814-825.
14 G.L. Luque, M.I. Rojas, E.P.M. Leiva, *Electrochimica Acta*, 2010, **56**, 523-530.
15 A.J. Stone, D.J. Wales, *Chem. Phys. Lett.*, 1986, **128**,501-503.
16 P. Giannozzi et al, *J. Phys.: Condens. Matter*, 2009, **21** 395502-21.
17 J.P. Perdew, K. Burke, M. Ernzerhof, *Phys. Rev. Lett.*, 1996, 77 3865.
18 L. Kleinman, D.M. Bylander, *Phys. Rev. Lett.*, 1982, **48** 1425.
19 H.J. Monkhorst, J.D. Pack, *Phys. Rev. B.*, 1976, **13**, 5188.
20 Y. Bu, Z. Chen, J. Yu, W. Li, *Electrochimica Acta*, 2013, **88**, 294-300.
21 N.W. Ashcroft, N.D. Mermin, Solid State Physics, United States, 1976, p. 96 ff.
22 Q. Guo, Y. Xie, X. Wang, S. Lv, T. Hou, X. Liu, *Chem. Phys. Lett.,* 2003, **380**, 84-87.
23 Y. Yuan, L. Zhang, J. Xing, M.I. Utama, X. Lu, K. Du, Y. Li, X. Hu, S. Wang, A. Genç, R. Dunin-Borkowski, J. Arbiol, Q. Xiong, *Nanoscale*, 2015, **7**, 12343-12350.
24 X. Zhang, X.Xie, H. Wang, J. Zhang, B. Pan, X. Xie, *J. Am. Chem. Soc.*, 2013, **135**, 18-21.
25 J. Tian, Q. Liu, A.M. Asiri, A.O. Al-Youbi, X. Sun, *Anal. Chem.*, 2013, **85**, 5595-5599.
26 D. Das, S.L. Shindle, K.K. Nanda, *ASC Appl. Mate. Interfaces*, 2016, **8,** 2181-2186.
27 A.J. Bard, L.R. Faulkner, Electrochemical Methods. Fundamentals and Applications, John Wiley and Sons (1980), Chap. 5.
28 N. Nasirizadeh, Z. Shekari, A. Nazari, M. Tabatabaee, *Journal of Food and Drug Analysis*, 2016, **24**, 72-82.
29 M.I. Rojas, M.J. Esplandiu, L.B. Avalle, E.P.M. Leiva, V.A. Macagno, *Electrochimica Acta*, 1998, **43**, 1785-1794.
30 B. Hirschorn, M.E. Oranzem, B. Tribollet, V. Vivier, I. Frateur, M. Musiani, *ElectrochimicaActa*, 2010, **55**, 6218-6227.
31 B.Y. Chan, S.M. Park, *Annu. Rev. Anal. Chem.*, 2010, **3**, 207-229.
32 X. Yuan, C. Song, H. Wang, J. Zhang, Electrochemical Impedance Spectroscopy in PME Fuel Cells: Fundamentals and Applications, Springer-Verlag, London 2010, p. 140-142.
33 X.H. Li, M. Antonietti,*Chem.Soc.Rev.*, 2013, **42**, 6593-6604.
34 X.H. Li,J.S. Chen, X. Wang, J. Sun, M. Antonietti,*J. Am. Chem. Soc.*, 2011, **133**, 8074-8077.
35 N. Sato,Electrochemistry at Metal and Semiconductor Electrodes, Elsevier, Amsterdam1998.
36 X.Li, Y. Dai, Y. Ma, S. Han, B. Huang, *Phys. Chem. Chem. Phys.*, 2014,**16**, 4230-4235.
37 John McMurry, Organic Chemistry, 8° Edition, Cengage Learning, México 2012, pp. 976.
38 T.L. Hill, Introduction to Statistical Thermodynamics, Dover Publication, Inc., New York 1986, p. 124-130.

Nanoscale Accepted Manuscript

This journal is © The Royal Society of Chemistry 2017